LAWRENCE
LIVERMORE
NATIONAL
LABORATORY

LLNL-JRNL-600276

Growth Rate Measurements of Phase Change Materials with Photo-Emission Electron Imaging During Laser Crystallization

M. K. Santala, B. W. Reed, S. Raoux, T. Topuria, T. LaGrange, G. H. Campbell

November 9, 2012

Applied Physics Letters

Disclaimer

GROWTH RATE MEASUREMENTS OF PHASE CHANGE MATERIALS WITH PHOTO-EMISSION ELECTRON IMAGING DURING LASER CRYSTALLIZATION

M.K. Santala*
Condensed Matter and Materials Division, Lawrence Livermore National Laboratory, Livermore, CA 94551, USA
santala1@llnl.gov, tel: +1 925-423-2968

B.W. Reed
Condensed Matter and Materials Division, Lawrence Livermore National Laboratory, Livermore, CA 94551, USA
reed12@llnl.gov, tel: +1 925-423-3617

S. Raoux
IBM T. J. Watson Research Center, Yorktown Heights, NY 10598, USA
simoner@us.ibm.com, tel: +1 914-945-1656

T. Topuria
IBM Research Division, Almaden Research Center, San Jose, CA 95120, USA
teyat@us.ibm.com, tel: +1 408-927-2922

T. LaGrange
Condensed Matter and Materials Division, Lawrence Livermore National Laboratory, Livermore, CA 94551, USA
lagrange2@llnl.gov, tel: +1 925-424-2383

G.H. Campbell
Condensed Matter and Materials Division, Lawrence Livermore National Laboratory, Livermore, CA 94551, USA
campbell7@llnl.gov, tel: +1 925-423-8276

Knowledge of crystallization kinetics is critical to the understanding of phase transformations in solids, including the crystallization of amorphous phase change materials used for optical and resistive memory applications. When such phase transformations are highly driven, as in laser- or current-induced crystallization at temperatures far above the onset of crystallization, the kinetics and the associated changes in microstructure are difficult to probe experimentally. At such high temperatures, competition between entropic and kinetic effects yields a maximum crystal growth rate, which cannot be reliably extrapolated from conventional low temperature data where growth progresses on the scale of nm/s. We use nanosecond-scale time-resolved microscopy with intense electron pulses to measure crystal growth rates in amorphous GeTe during laser crystallization. Crystallization, driven by heating rates of ~10^{10} K/s, was captured in multi-frame movies and crystal growth speeds exceeding 3 m/s were measured. Observed changes in growth rate during crystallization along with models of the laser-specimen interactions and crystal growth rate indicate that observed crystallization occurs at temperatures close to and slightly above where the maximum growth rate is achieved.

Optical memory (CDs, DVDs) and non-volatile Random Access Memory (RAM) exploit the distinct optical and electrical properties of the amorphous and crystalline phases of chalcogenide-based phase change materials (PCMs). For memory applications, it must be possible to switch between the amorphous and crystalline phases in nanoseconds by rapid heating.[1] Heating may be achieved by laser- or current-pulses, but in either case, crystallization of the amorphous phase is the slower, data-rate-limiting process compared to the melt-quenching process that switches the material from crystalline to amorphous. Thus a solid understanding of crystallization kinetics during laser and resistive heating, where heating rates may exceed 10^{10}

K/s and crystal growth rates approach their maximum, are of vital interest for PCMs as they directly impact device switching speed.

Here we study crystallization of GeTe, a PCM that is attractive for both high temperature and non-volatile RAM applications because of its high crystallization temperature, T_x,[2,3] and rapid switching speed.[3,4] Crystallization occurs rapidly in stoichiometric GeTe,[4,5] because the amorphous and crystalline phases have identical composition, and a partitionless transformation occurs.[5,6] Laser crystallization of amorphous GeTe has been monitored on the nanosecond scale by measuring changes in optical and electrical properties,[4,6-8] but with these methods, only the overall fraction crystallized is extracted. Consequently the nucleation and growth rates cannot be independently measured, even though they both impact the overall crystallization rate.

Microscopic techniques that image microstructural changes can be used to study nucleation and growth independently, but these techniques are severely limited in their temperature range due to limits in the range of experimentally measurable growth rates. Growth rates have been measured with optical microscopy[9-11] and transmission electron microscopy (TEM)[12] near the crystallization temperature, T_x, which varies with heating rate but has been taken as ~450 K.[2,5] Consequently crystal growth rates for GeTe discussed in the literature[9-12] have only been measured over a small temperature range, 393 to 453 K. The crystal growth of GeTe and other PCMs is sometimes described as linear in time and having an Arrhenius dependence for isothermal measurements near T_x.[9-12] While adequate for low temperatures, this model cannot predict growth rates at higher temperatures, as it accounts for neither the diminishing driving force for crystallization when approaching the melting temperature, T_m (997 K for GeTe[13]), nor the strong temperature dependence of the atomic transport coefficients.[14,15] If we assume, as is commonly done,[16] that the amorphous material relaxes into a supercooled liquid as it approaches

T_m, then the entropic term in the Gibbs free energy change reduces the driving force (and hence the crystallization rate) to zero at T_m, thus implying a maximum growth rate at some intermediate temperature. Kelton and Greer developed a growth rate model for glass-forming systems applicable up to T_m,[17,18] but the expected maximum growth rates for GeTe and similar PCMs (on the order of m/s) are much too high to be captured with conventional experimental techniques.

The need to better understand crystallization kinetics during laser- and Joule-heating motivates direct experimental measurements of the growth rate under high heating rates and temperatures far above T_x. We study kinetics of crystallization of amorphous GeTe using pulsed electron imaging, which enables direct measurement of growth rates during laser crystallization. This is achieved with the dynamic TEM (DTEM),[19] a TEM that has been modified to enable controlled photoemission of intense electron pulses used for nanosecond-scale imaging and diffraction of irreversible processes. With this instrument, a transformation is initiated in a specimen with a laser pump pulse. Multiple pulses from a second laser, timed against the pump laser in an operator-defined delay, strike the TEM cathode inducing emission of ~10^9 electrons over several nanoseconds. Up to nine electron pulses may be spaced over several microseconds, probing the specimen multiple times during a single initiated reaction, forming a movie of an *irreversible* reaction. Here, each electron pulse is 17.5 ns, defining the temporal resolution of the experiment. The DTEM has been used to probe phase transformations in $Ge_2Sb_2Te_5$,[20] metals,[21-23] and semiconductors,[24] but in previous experiments the reacting specimen was probed with a single electron pulse. The design of the DTEM "single-shot" mode[25] and the modifications that have enabled the current "movie" mode operation[26] have been described elsewhere.

Regions of a 30 nm GeTe film on an amorphous 20 nm silicon nitride membrane were crystallized with a single 1064 nm wavelength laser pulse with a 135±5-μm $1/e^2$ diameter, a 12-

ns FWHM duration, and a total energy from 5.1 to 5.5 μJ. Figure 1 shows two series of nine 17.5-ns images during crystal growth at the center of the laser-affected areas. The nucleation rate is low at the hottest part of the specimen, and the grains grow many microns in diameter before impingement, consistent with growth-dominated crystallization expected for GeTe.[4] Due to the stochastic nature of nucleation, the microstructural development during crystallization unfolds differently in the two examples. In Figure 1a, many grains grow inward from the periphery where the temperature was initially lower and the nucleation rate higher, whereas in Figure 1b, a single grain grows and is not impinged within the field of view by 2590 ns. The crystal growth rates as a function of delay after the specimen laser shot is shown in Figure 2. In the first few hundred nanoseconds the growth rate exceeds 3 m/s with a drop in rate as time progresses.

To understand the change of growth rate with time and to relate our data to growth rates measured below T_x, it is necessary to connect our growth rates to temperature, rather than laser energy. Direct temperature measurements are not generally experimentally accessible for laser heating experiments, but temperatures may be modeled, e.g. [6,20]. Spatio-temporal temperature profiles were developed using finite element analysis (FEA) modeling of laser-specimen interactions and heat flow. The temperature at various positions is shown as a function of time in Figure 3 for laser heating of the specimen in our experiment. The temperature rises rapidly during the peak intensity of the laser pulse, exceeding 10^{10} K/s at the center of the laser spot, and large spatial temperature gradients are established within 30 ns. The specimen has a large, thin electron-transparent area and due to this geometry, the temperature gradients persist for many microseconds. In the time window of the growth rate measurements (120 to 2590 ns) the local temperature established by laser heating is essentially isothermal, thus these experiments lend themselves well to comparison with isothermal growth rate measurements near T_x.[9-12] Due to low

nucleation rates and long incubation times, no significant amount of amorphous GeTe crystallizes within the 15-ns laser pulse, therefore transformation to the crystalline phase is not expected to affect the laser absorption, but it will affect the temperature profile later due to the heat of crystallization released and higher thermal conductivity of the crystalline phase. The simulations shown do not include changes in material properties due to phase transformations, but in simulations with the higher thermal conductivity of crystalline GeTe only a very slightly more rapid decay of the temperature profile occurs within 3 μs. Heating due to enthalpy of crystallization will be highly localized in the time-scale of the experiment and the pattern of heating will depend sensitively on the course of nucleation and growth, which will unfold differently in each specimen. Given the magnitude of the enthalpy of crystallization and heat capacity of the GeTe and support, local heating up to ~180K could occur near the crystallization front. The temperatures near the center of the laser spot may locally approach T_m and indeed evidence of melting and dewetting of the film occurs where the grains impinge in Figure1a. If we do take this as evidence that the center of the laser spot is heated by the laser to a temperature between T_m - 180K and T_m, then this verifies the calculated laser absorption in Figure 3 within an error bound of order 10%.

We consider our measurements (at temperatures approaching T_m) and those from the literature (near or below T_x),[9-12] in the context of Kelton and Greer's growth rate model.[17,18] We extend their analysis for the growth of a spherical super-critical crystal in an amorphous matrix[17,18] to growth of a cylindrical cluster in a thin film, which is applicable here. The growth rate then has the form:

$$v_G = -\left(\frac{6V}{\pi}\right)^{\frac{1}{3}} \frac{8D}{\lambda^2} \operatorname{Sinh}\left\{\frac{V}{2k_BT}\left[\Delta G_V + \frac{\gamma_{ac}}{R} + \frac{1}{d}\left(\gamma_{xs} - \gamma_{as} + \gamma_{xc} - \gamma_{ac}\right)\right]\right\} \quad (1)$$

which depends on the volume of a monomer, V; atomic diffusivity, D; jump distance at the

interface, λ; temperature, T; change in bulk free energy on crystallization, ΔG_V; cluster radius, R; film thickness, d; interfacial energy between crystalline and amorphous GeTe, γ_{ax}, as well as interfacial energies of those phases with the substrate and capping layer, γ_{as}, γ_{xs}, γ_{ac}, and γ_{xc}. Details on the derivation of equation (1) are in the Supplementary material. Approaching T_m, growth is limited by the diminishing thermodynamic driving force and below T_x it is limited by diminishing atomic diffusivity, D.

A calculated growth rate, v_G, from Equation (1), along with growth rate data for GeTe,[9-12] is plotted in Figure 4. ΔG_V is given the form $\Delta G_V = \frac{\Delta H(T_m - T)}{T_m}\left(\frac{2T}{T_m + T}\right)$, where ΔH, the enthalpy of crystallization, is taken from calorimetric data.[27] Data on diffusivity over a broad range of temperatures are available for few systems and are scant for GeTe, thus we make assumptions regarding the atomic mobility as described below. Importantly, we expect the temperature dependence of the atomic mobility to be different at low temperatures where the material is a glass, than at high temperature where it is a supercooled liquid. A glass transition temperature, T_g, has not been measured for GeTe, but it is expected to be close to T_x in PCM alloys. Both calculated values of T_g[28] and trends in experimentally measured T_x and T_g of Ge_xTe_{1-x} alloys[29] suggest that $T_g > T_x$. At temperatures near T_x where solid state behavior is expected, D(T) is given an Arrhenius dependence. The activation energy for D is taken as the average of activation energies for growth in references [9-12]; since ΔG_V is large but slowly varying below T_x this activation energy should reflect the temperature dependence of the atomic mobility. Note that this dependence for D(T) in equation (1), when fitted to the available low temperature growth data,[9-11,12] would lead to a gross over-estimate of the growth rate at higher temperatures (exceeding 1 km/s for a 10 nm grain). At higher temperatures, we use the Vogel-Fulcher-Tammann (VFT) relation, $\eta = \eta_o \exp(\frac{B}{T - T_o})$, to describe η(T) and the Einstein-Stokes relation to

relate viscosity to diffusivity. Viscosity data are available for liquid GeTe for only two temperatures above T_m,[30] which does not fully constrain the VFT relation. We take T_o, which affects the low temperature drop off in atomic mobility (also creating a rapid drop in growth rate), to be $0.4T_m$, placing the transition from glassy to liquid behavior, the kink in the plot, slightly above T_x, as expected.[29] The values of η_o and B, are then constrained by the available viscosity data.

Based on the observed reduction in growth rate and the expected local increase in temperature due to the enthalpy of crystallization, we conclude that we are operating in the temperature range where an increase in temperature of >100 K leads to a only small reduction in growth rate (shaded region in Figure 4). These photoemission transmission electron movies with nanosecond-scale time resolution yield direct measurement of PCM growth rates where they achieve their maximum, which is especially relevant to the function of PCM memory devices.

Thus DTEM experiments are valuable for the evaluation of PCM alloys *in the technologically relevant temperature regime*, but further opportunities exist to build a more complete understanding of crystallization kinetics in GeTe and other PCMs. There remains a gulf between the growth rate measurements made with conventional microscopy below T_x and our experiments. In this intermediate region, growth rates still span many orders of magnitude and the nucleation rate achieves its maximum. Recently, this intermediate regime was probed with ultrafast-heating calorimetry in a related PCM, $Ge_2Sb_2Te_5$.[15] Although calorimetry can not yield absolute values of growth rates, those experiments began to reveal temperature dependency of crystal growth rate in a PCM above T_x. Photoemission TEM may also be used to measure growth rates just above T_x, where crystal growth is too fast to be captured with conventional techniques, and where the transition from amorphous solid to supercooled liquid occurs. At these

temperatures, high spatial resolution will be required because of high nucleation rates, but the required temporal resolution will be relaxed because of somewhat lower growth rates. Photo-emission electron microscopy using microsecond pulses, which has the potential to achieve atomic resolution,[25] can be applied in this regime. No other technique with the ability to visualize microstructural changes during irreversible reactions has approached this level of spatial and temporal resolution. We are moving toward a time when we may use electron microscopy not only to locate exactly where atoms are, but perhaps more importantly, where they are going.

Our photoemission TEM experiments have already yielded quantitative measure of growth rate close to T_m where GeTe is a supercooled liquid, revealing transformations of microstructure in states of matter inaccessible at lower heating rates and other characterization techniques. These experiments, coupled with appropriate models of crystal growth, provide a path to better understanding of crystal growth in GeTe and other PCMs. A fundamental understanding of crystal growth, which is benchmarked by the ability to accurately model experimental observations over a wide range of conditions, will help advance designs for new memory applications.

Methods

The DTEM was used to image crystallization of an as-deposited amorphous film of 30 nm GeTe on a Si support with a 20 nm thick, 0.25 x 0.25 mm amorphous silicon nitride window. GeTe films were deposited at room temperature using magnetron sputtering. A target with a nominal composition of Ge:Te = 50:50 atomic % was used. Rutherford backscattering revealed the film composition to be Ge 50.7 ± 0.5 atomic % and Te 49.3 ± 0.5 atomic %. The DTEM specimen pump laser used to induce crystallization is a Nd:YAG laser (1064 nm wavelength, 135±5-μm $1/e^2$ diameter, 12-ns FWHM pulse duration). Crystallization was induced with 4.8 or 5.3 μJ pulses. The higher energy caused the growth of large grains (>1 μm) at the center of the laser spot. Photo-emitted electron pulses were generated with a Nd:YAG laser converted to 5^{th} harmonic (213 nm) directed onto the TEM cathode. The electron probe pulses and pump laser were aligned such that the imaging of the specimen occurred where the specimen receives the greatest laser intensity. Bright field images of each initiated reaction were generated from a series of nine 17.5 ns electron pulses. The nine images were captured in a single "exposure" of the CCD camera through the use of an electrostatic deflector that shifts each electron image to a different part of the detector. Growth rates were determined by tracking the position of crystallization fronts in each frame of the nine-frame movie series. The error in determining the position of the crystallization front is estimated to be ±60nm. The rate at each delay in Figure 2 represents the amount the crystalline front has advanced in the time interval since the previous image. Measurements were made at evenly spaced intervals normal to the crystal/amorphous interface at the earlier delay (every ~240 nm). The number of measurements varied (between 5 and 36) depending on the length of the crystalline/amorphous interface visible in the field of view at each delay.

Finite element analysis: The laser interactions and heat flow were simulated in a commercial finite element package, COMSOL™. Laser-specimen interactions, which include specimen geometry and materials properties as well as wavelength and polarization of the incident laser, were modeled in a time-harmonic study. The incident light was taken to be a uniform plane wave incident at 42°. This plane wave served as the source term in a standard scattered-wave electrodynamics calculation. The total dissipative losses in the materials in the laser-specimen interaction simulation were used as the heat source in a heat transport simulation. To save on computational time, a 2D model was used and the Si frame was truncated relative to the experimental set-up. The model dimensions are large enough that changes in the dimension do not significantly affect the absorption and temperature profiles in the area of interest. The simulation region was bounded by perfectly matched layers, which impose the boundary condition that no waves apart from the specified source term were inbound from outside the region. For the heat transport simulation, the heat source was given a spatially varying envelope reflecting the size (135um $1/e^2$ dia.) and shape (Gaussian) of the laser spot and time-dependent envelope reflecting the temporal profile of the DTEM specimen laser (Gaussian pulse centered at 15 ns, 12-ns FWHM) forming a heat source, which was scaled such that the total laser energy in the shaped pulse matched the experimental values. It is assumed heat diffusion through the solid is the most significant path for heat flow; radiative losses were included in some models, but, as expected, were insignificant compared to diffusion through the solid. Materials properties were taken from the available literature and were generally treated as temperature independent; phase transformations were not included in the simulation presented here.

Acknowledgements

This work performed under the auspices of the U.S. Department of Energy, Office of Basic Energy Sciences, Division of Materials Sciences and Engineering by Lawrence Livermore National Laboratory under Contract DE-AC52-07NA27344.

Author Contributions

M.S. designed and M.S. and T.L. performed the transmission electron microscopy experiments. S.R. and T.T. provided technical expertise on materials, deposited experimental films, and conducted initial assessment of the samples. M.S., B.R. and G.C. analyzed the results. M.S. and B.R. performed finite element analysis simulations. B.R., T.L., and G.C. gave technical and/or conceptual advice on the electron microscopy experiments. M.S. prepared the manuscript. All authors reviewed and commented on the manuscript.

Additional Information

The authors declare no competing financial interests.

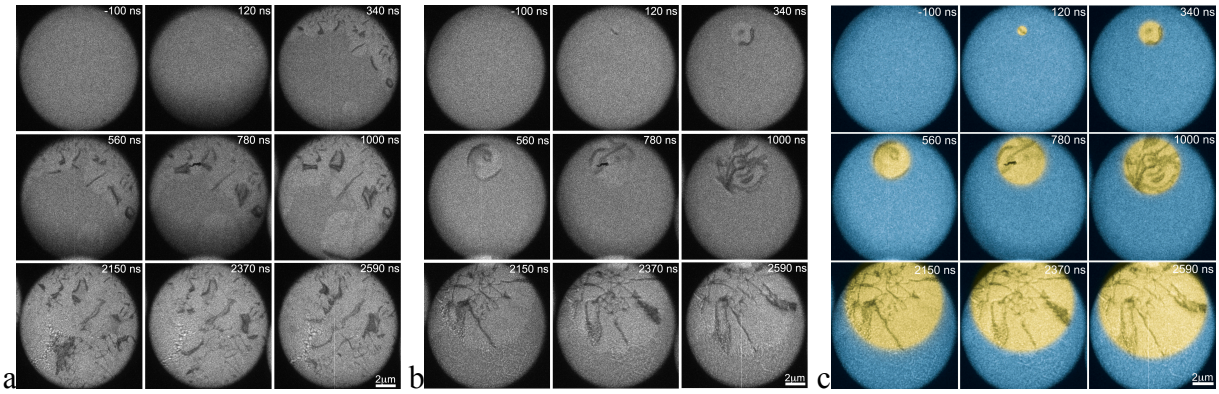

Figure 1 (a-b) GeTe films in series of 17.5-ns images during crystal growth after two different 5.3 μJ laser shots. Time signatures are relative to the time of the peak specimen laser intensity with an uncertainty of ±3 ns. Image (c) adds false color to image (b) to clarify the growing crystalline region.

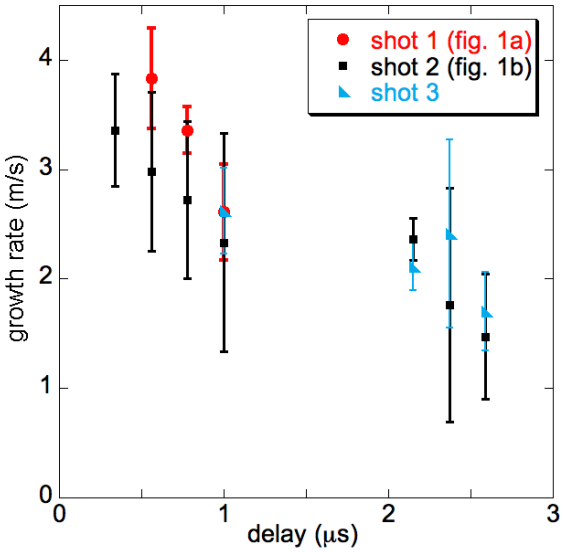

Figure 2 (a) Growth rate versus delay after specimen laser shot. The rate given at each delay represents the amount the crystalline front has advanced in the time interval since the previous image. Rates are averaged over evenly spaced measurements normal to the crystal/amorphous interface; bars indicate the sample standard deviation.

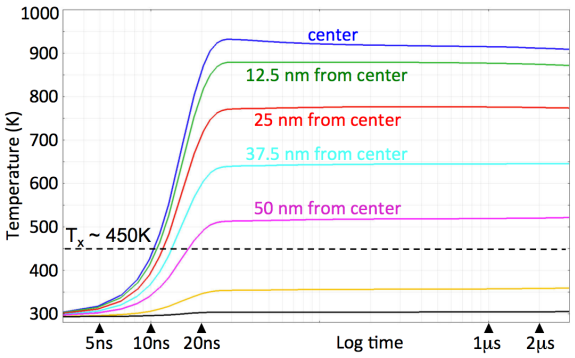

Figure 3 Simulated temperature profiles in a GeTe film for a laser pulse centered in a 250 μm TEM grid window for a 5.3 μJ laser pulse. The heating rate exceeds 10^{10} K/s at the peak of the laser pulse at 15 ns; after the laser pulse the local temperature remains steady for microseconds.

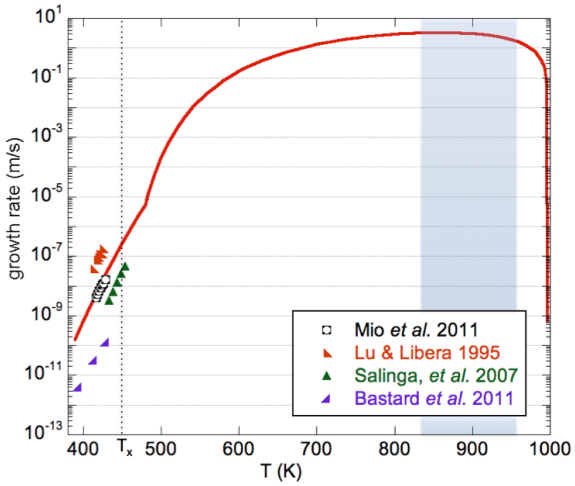

Figure 4 Growth rate vs. temperature showing data points from conventional TEM and optical microscopy experiments and equation (1) (solid line). Our experiments measure growth rates of GeTe in the shaded where a slight rate drop in rate is expected due to a local increase in temperature cause by heat of devitrification released.

REFERENCES

1. Raoux, S. & Wuttig, M., *Phase Change Materials: Science and Applications*. (Springer Verlag, Berlin, 2008).

2. Raoux, S., Munoz, B., Cheng, H.-Y., & Jordan-Sweet, J.L., Phase transitions in Ge-Te phase change materials studied by time-resolved x-ray diffraction. *Appl. Phys. Lett.* **95**, 143118 (2009).

3. Bruns, G. *et al.*, Nanosecond switching in GeTe phase change memory cells. *Appl. Phys. Lett.* **95**, 043108 (2009).

4. Raoux, S., Cheng, H.Y., Caldwell, M.A., & Wong, H.S.P., Crystallization times of Ge-Te phase change materials as a function of composition. *Appl. Phys. Lett.* **95**, 071910 (2009).

5. Chen, M., Rubin, K.A., & Barton, R.W., Compound materials for reversible, phase-change optical-data storage. *Appl. Phys. Lett.* **49**, 502-504 (1986).

6. Huber, E. & Marinero, E.E., Laser-induced crystallization of amorphous GeTe - a time resolved study. *Phys. Rev. B* **36**, 1595-1604 (1987).

7. Libera, M. & Chen, M., Time-resolved reflection and transmission studies of amorphous Ge-Te thin-film crystallization. *J. Appl. Phys.* **73**, 2272-2282 (1993).

8. Gawelda, W. *et al.*, Dynamics of laser-induced phase switching in GeTe films. *J. Appl. Phys.* **109**, 123102 (2011).

9. Lu, Q.M. & Libera, M., Microstructural measurements of amorphous GeTe crystallization by hot-stage optical microscopy. *J. Appl. Phys.* **77**, 517-521 (1995).

10. Mio, A.M. *et al.*, Nucleation and grain growth in as deposited and ion implanted GeTe thin films. *Journal of Non-Crystalline Solids* **357**, 2197-2201 (2011).

11. Salinga, M. *et al.* Glass Transition and Crystallization in Phase Change Materials in *European\Phase Change and Ovonics Symposium* (2007).

12. Bastard, A. *et al.*, Crystallization study of "melt quenched" amorphous GeTe by transmission electron microscopy for phase change memory applications. *Appl. Phys. Lett.* **99**, 243103 (2011).

13. Schlieper, A. & Blachnik, R., Calorimetric investigations of liquid Ge-Te and Si-Te alloys. *J. Alloy. Compd.* **235**, 237-243 (1996).

14. Kalb, J.A., Spaepen, F., & Wuttig, M., Kinetics of crystal nucleation in undercooled droplets of Sb- and Te-based alloys used for phase change recording. *J. Appl. Phys.* **98**, 054910 (2005).

15. Orava, J., Greer, A.L., B., G., Hewak, D.W., & Smith, C.E., Characterization of supercooled liquid $Ge_2Sb_2Te_5$ and its crystallization by ultrafast-heating calorimetry. *Nat. Mater.* **11**, 279-283 (2012).

16. Turnbull, D., Under what conditions can a glass be formed? *Contemporary Physics* **10**, 473-488 (1969).

17. Kelton, K.F. & Greer, A.L., Interpretation of experimental measurements of transient nucleation in *Rapidly Quenched Metals*, edited by S. Steeb & H. Warlimont (Elsevier Science Publishers B.V., Würzburg, 1985), Vol. 1, pp. 223-226.

18. Kelton, K.F. & Greer, A.L., Transient nucleation effects in glass-formation. *Journal of Non-Crystalline Solids* **79**, 295-309 (1986).

19. LaGrange, T. *et al.*, Single-shot dynamic transmission electron microscopy. *Appl. Phys. Lett.* **89**, 004105 (2006).

20. Santala, M.K. *et al.*, Nanosecond *in situ* transmission electron microscope studies of the reversible $Ge_2Sb_2Te_5$ crystalline ⇔ amorphous phase transformation. *J. Appl. Phys.* **111**, 024309 (2012).

21. Kim, J.S. *et al.*, Imaging of transient structures using nanosecond in situ TEM. *Science* **321**, 1472-1475 (2008).

22. Kulovits, A., Wiezorek, J.M.K., LaGrange, T., Reed, B.W., & Campbell, G.H., Revealing the transient states of rapid solidification in aluminum thin films using ultrafast in situ transmission electron microscopy. *Philosophical Magazine Letters* **91**, 287-296 (2011).

23. LaGrange, T. *et al.*, Strongly driven crystallization processes in a metallic glass. *Appl. Phys. Lett.* **94**, 184101 (2009).

24. Nikolova, L. *et al.*, Nanocrystallization of amorphous germanium films observed with nanosecond temporal resolution. *Appl. Phys. Lett.* **97**, 203102 (2010).

25. Armstrong, M.R. *et al.*, Practical considerations for high spatial and temporal resolution dynamic transmission electron microscopy. *Ultramicroscopy* **107**, 356-367 (2007).

26. Reed, B.W. *et al.*, The Evolution of Ultrafast Electron Microscope Instrumentation. *Microscopy and Microanalysis* **15**, 272-281 (2009).

27. Schlieper, A., Feutelais, Y., Fries, S.G., Legendre, B., & Blachnik, R., Thermodynamic evaluation of the germanium-tellurium system. *Calphad-Computer Coupling of Phase Diagrams and Thermochemistry* **23**, 1-18 (1999).

28. Lankhorst, M.H.R., Modelling glass transition temperatures of chalcogenide glasses. Applied to phase-change optical recording materials. *Journal of Non-Crystalline Solids* **297**, 210-219 (2002).

29. Sarrach, D.J., DeNeufville, J.P., & Haworth, W.L., Studies of amorphous Ge-Se-Te alloys (1): preparation and calorimetric observations. *Journal of Non-Crystalline Solids* **22**, 245-267 (1976).

30. Herwig, F. & Wobst, M., Investigations on the viscosity of liquid Ge-Te alloys. *Zeitschrift Fur Metallkunde* **82**, 917-920 (1991).

Supplement to:

GROWTH RATE MEASUREMENTS OF PHASE CHANGE MATERIALS WITH PHOTO-EMISSION ELECTRON IMAGING DURING LASER CRYSTALLIZATION

M.K. Santala,[1] B.W. Reed,[1] S. Raoux,[2] T. Topuria,[3] T. LaGrange,[1] and G.H. Campbell[1]

[1]Condensed Matter and Materials Division, Lawrence Livermore National Laboratory, Livermore, CA 94551, USA
[2]IBM T. J. Watson Research Center, Yorktown Heights, NY 10598, USA
[3]IBM Research Division, Almaden Research Center, San Jose, CA 95120, USA

MODEL FOR CRYSTAL GROWTH RATE IN AN AMORPHOUS THIN FILM

To model the growth of crystalline GeTe into an amorphous film, we follow the approach used for glass-forming materials described by Kelton and Greer[1,2] for the growth of a super-critical crystalline cluster in an amorphous matrix. We modified their analysis to take into consideration the specimen geometry for growth of crystalline clusters in thin films sandwiched between a substrate and a capping layer (or air), which is the geometry of interest for many applications of phase change materials and is the geometry generally used for the study of crystallization of phase change materials. The geometry is shown here:

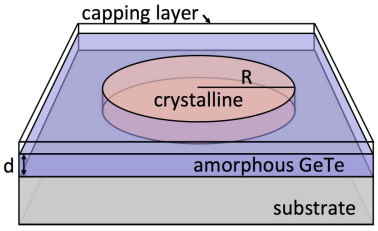

A simplifying assumption was made that the growing grain is a right cylinder, although in reality, the contact angle of the grain at the substrate and capping layer will depend on the relative interfacial energies between the different phases.

Kelton and Greer use reaction rate theory to find the reaction rate for which a super-critical cluster of *n* molecules gains a new molecule. They give an average rate at which a crystalline cluster gains a monomer as:

$$\frac{dn}{dt} = \frac{6D}{\lambda^2} O_n \{\exp\left[\frac{\Delta G(n) - \Delta G(n+1)}{2k_B T}\right] - \exp\left[\frac{\Delta G(n+1) - \Delta G(n)}{2k_B T}\right]\} \qquad \text{(i)}$$

where D is the atomic diffusivity at the crystal-amorphous interface, λ is the jump distance across the interface, O_n is number of sites on the cluster surface (which for the above geometry is $O_n = \sqrt{\frac{16nd}{3R}}$), d is the film thickness and R is the radius of the growing crystal. *T* is the temperature and k_B takes its usual meaning of Boltzmann's constant.

For the thin film geometry, the change in free energy from an addition to the cluster, ΔG, contains both the bulk free energy and the interfacial energy, and when written in terms of a cluster size a radius R is given by:

$$\Delta G = \pi R^2 d \Delta G_V + 2\pi R d \gamma_{ax} + \pi R^2 [(\gamma_{xs} - \gamma_{as}) + (\gamma_{xc} - \gamma_{ac})] \qquad \text{(ii)}$$

where ΔG_V is the change in the bulk free energy on crystallization per unit volume. The terms γ_{ax}, γ_{xs}, γ_{as}, γ_{xc}, and γ_{ac} are interfacial energies, where the subscripts indicate the relevant phases: "a" for amorphous matrix, "x" for crystalline grain, "s" for substrate, and "c" for capping layer. The second term on the right side of equation (ii) is the energetic barrier to growth caused by increasing the interfacial area of the growing crystal with the amorphous matrix. The third term accounts for the change in interfacial energy at the substrate and capping layer interfaces during crystal growth and is sensitive the differences (γ_{xs} -γ_{as}) and (γ_{xc} - γ_{ac}), rather than the absolute values of the individual interfacial energies.

Taking each of the *n* monomers to have an the effective monomer volume, *V*, equations (i) and (ii) may be combined to find the growth rate:

$$v_G = \frac{dR}{dt} = -\left(\frac{6V}{\pi}\right)^{\frac{1}{3}} \frac{8D}{\lambda^2} \mathrm{Sinh}\left\{\frac{V}{2k_B T}\left[\Delta G_V + \frac{\gamma_{ax}}{R} + \frac{1}{d}\left((\gamma_{xs} - \gamma_{as}) + (\gamma_{xc} - \gamma_{ac})\right)\right]\right\} \qquad \text{(iii), eqn (1) main text}$$

For figure 4 in the main text, an estimate of the interfacial energy between the GeTe amorphous and crystalline phases was made based on the interfacial energies extracted by Kalb *et al*.[3] from their calorimetric data on Ge_4SbTe_5 (0.047 ± 0.06 J/m^2) and $Ge_2Sb_2Te_5$ (0.40 ± 0.03 J/m^2). This assumes homogeneous nucleation, and thus is a lower bound to the true interfacial energy. We use 0.047 J/m^2 as an estimate for γ_{ax}. We also take the differences (γ_{xs} -γ_{as}) + (γ_{xc} - γ_{ac}) to be 0.0005 J/m^2 but note that physically reasonable changes to the values of the interfacial energies make little difference when plotted on the scale of figure 4 for R > 10nm. In both our experiments and the growth rate experiments on GeTe performed with optical microscopy4-6, the grain radii exceeded 1 μm. Over the range covered by figure 4, equation (iii) is most strongly affected by ΔG_V(T) and D(T).

REFERENCES

1. Kelton, K.F. & Greer, A.L., Interpretation of experimental measurements of transient nucleation in *Rapidly Quenched Metals*, edited by S. Steeb & H. Warlimont (Elsevier Science Publishers B.V., Würzburg, 1985), Vol. 1, pp. 223-226.

2. Kelton, K.F. & Greer, A.L., Transient nucleation effects in glass-formation. *Journal of Non-Crystalline Solids* **79**, 295-309 (1986).

3. Kalb, J.A., Spaepen, F., & Wuttig, M., Kinetics of crystal nucleation in undercooled droplets of Sb- and Te-based alloys used for phase change recording. *J. Appl. Phys.* **98**, 054910 (2005).

4. Lu, Q.M. & Libera, M., Microstructural measurements of amorphous GeTe crystallization by hot-stage optical microscopy. *J. Appl. Phys.* **77**, 517-521 (1995).

5. Mio, A.M. *et al.*, Nucleation and grain growth in as deposited and ion implanted GeTe thin films. *Journal of Non-Crystalline Solids* **357**, 2197-2201 (2011).

6. Salinga, M. *et al.* Glass Transition and Crystallization in Phase Change Materials in *European\Phase Change and Ovonics Symposium* (2007).